Myc determines the functional age state of oligodendrocyte progenitor cells

Björn Neumann[1]†, Michael Segel[1]†, Tanay Ghosh[1], Chao Zhao[1], Panagiotis Tourlomousis[2], Adam Young[1], Sarah Förster[1], Amar Sharma[1], Zi-Yu Chen[1], Juan Cubillos[1], Khalil Rawji[1], Kevin J. Chalut[1,3] and Robin J.M. Franklin[1]*

[1]*Wellcome-Medical Research Council Cambridge Stem Cell Institute, Cambridge Biomedical Campus, University of Cambridge, Cambridge CB2 0AH, UK*

[2]*Department of Veterinary Medicine, University of Cambridge, Cambridge CB3 0ES, UK*

[3]*Department of Physics, University of Cambridge, Cambridge CB3 0HE, UK*

*Correspondence to: rjf1000@cam.ac.uk

†Contributed equally

ABSTRACT

Like many adult stem cell populations, the capacity of oligodendrocyte progenitor cells (OPCs) to proliferate and differentiate is significantly impaired with ageing. Previous work has shown that tissue-wide transient expression of the pluripotency factors Oct4, Sox2, Klf4 and c-Myc extends lifespan and enhances somatic cell function. Here we show that just one of these factors, c-Myc, is sufficient to determine the age state of the OPC: c-Myc expression in aged OPCs drives their functional rejuvenation, while inhibition of c-Myc in neonatal OPCs induces an aged-like phenotype, as determined by *in vitro* assays and transcriptome analysis. We show that increasing c-Myc expression specifically in aged OPCs *in vivo* restores their proliferation and differentiation capacity, thereby enhancing regeneration in an otherwise aged CNS environment. More generally, our results directly link Myc to cellular activity and cell age-state, with implications for understanding regeneration in the context of ageing and provide important insights into the biology of stem cell ageing.

In normal development, mammalian embryonic stem cells unidirectionally differentiate into adult somatic cells. During this process, cells progressively commit to the various lineages of the adult organism. In the adult, a reserve pool of tissue-specific adult stem cells, however, does not terminally differentiate. Instead, these cells remain undifferentiated and poised to differentiate into tissue-specific cell-types to maintain homeostasis or repair damaged tissue. In the CNS, the most widespread and abundant adult stem cell population is the oligodendrocyte progenitor cell (OPC). In adulthood, OPCs self-renew and give rise primarily to new myelinating oligodendrocytes, but can also generate astrocytes and Schwann cells [1]. OPCs remain actively cycling and differentiating well into adulthood [2,3]. However, with ageing, the capacity for OPCs to both self-renew and differentiate into myelinating oligodendrocytes is significantly impaired [4,5]. Adult OPCs become increasingly inefficient at regenerating new myelin forming oligodendrocytes in the spontaneous regenerative process of remyelination [6], a loss of function that is highly relevant for patients with the chronic demyelinating disease multiple sclerosis (MS).

Regardless of physiological age, adult cells can be reset to an embryonic state by the pluripotency factors Oct4, Sox2, Klf4, and c-Myc (OSKM factors). Expression of the OSKM factors erases all the cellular hallmarks of ageing [7]. More recently, it has been shown that short transient expression of OSKM factors will partially reprogram an aged cell to a younger more rejuvenated state, thereby extending lifespan and restoring the regenerative capacity of aged animals [8]. However, the role that each of the pluripotency factors play in the observed effects of partial reprogramming or indeed whether all or only some of the reprogramming factors are required for rejuvenation remains unknown.

In this study, we ask whether aged OPCs can be rejuvenated by partial reprograming, what factors are required to achieve this and whether this leads to enhanced myelin regeneration in the aging CNS.

RESULTS

c-Myc alone regulates age-state of adult OPCs

Transient over-expression of OSKM factors causes aged cells of several cell types to revert to a more functional youthful state [8,9]. To establish if this approach also works for oligodendrocyte progenitor cells, we transfected aged OPCs (>18 months old) with a single pulse of *in vitro* transcribed capped and polyadenylated mRNA with modified nucleotides (pseudo-UTP and 5-methyl-CTP) encoding eGFP or a polycistronic expression cassette encoding for OSKM, in which the individual genes are linked by 2A sequences (Fig. 1a, Extended Data Fig. 1a). Transfection of eGFP encoding mRNA into aged OPCs was highly efficient, with over 80% of OPCs expressing the gene after 48 hours (Extended Data Fig. 1b-c). We then assessed the ability of the aged OPCs to proliferate and differentiate, two processes for which the capacity of OPCs declines with increasing age [4,5]. We found that OSKM treatment was able to restore the ability of aged for proliferation 5 days after transfection determined by the incorporation of EdU (Fig. 1b,c). When switched into differentiation medium after 5 days OSKM-treated OPCs also differentiated more efficiently into MBP-positive oligodendrocytes (Fig. 1b, d). We concluded that a single transient burst of OSKM expression was able to restore the functional potential of aged OPCs (Fig. 1a).

Next, we asked if it was possible to use only one of these factors to achieve a similar effect (Fig. 1e). We hypothesized that the OSKM factors potentially capable of rejuvenating aged OPCs will be those expressed in neonatal OPCs, when OPCs have their highest generative potential. To address this, we isolated both primary aged (≥14 months) and neonatal (≤p7) rat OPCs by magnetic associated cell sorting (MACs) using the OPC marker A2B5 [4], and then used sequencing data from the two populations [5] to identify expression of the transcription factors *Sox2* and *c-Myc* in neonatal OPCs but not in aged OPCs (Fig. 1f). We excluded Oct4 from subsequent analysis as it is not expressed at any age-point in the OPC lifecycle, and Klf4 because it was not differentially expressed between neonate and aged OPCs. We confirmed the decrease of c-Myc expression in OPCs with ageing using a published scRNA-seq dataset [10] (Extended Data Fig. 1d) and by qPCR, measuring c-Myc mRNA levels in freshly isolated OPCs from neonatal and aged rats (Extended Data Fig. 1e). We then asked whether over-expression of *Sox2* and *c-Myc*, either in combination or individually, might partially re-program aged

OPCs. To accomplish this, aged OPCs were plated in high concentrations of growth factors, PDGF-AA and bFGF, to induce proliferation, which occurs at low levels in cultures of aged OPCs [5]. Twenty-four hours after plating, the aged OPCs were transfected with *in vitro* transcribed modified mRNAs encoding *eGFP*, *Sox2*, *c-Myc*, or a combination of *Sox2* and *c-Myc* (Fig. 1g). We found high levels of proliferation of aged OPCs in the *Sox2* and *c-Myc* transfected conditions, but a much less pronounced effect when only *Sox2* was transfected (Extended Data Fig. 1f). *c-Myc* overexpression alone recapitulated the effect of combined Sox2 and c-Myc treatment: 4 days after 1 round of transfection of Myc, 18-month-old OPCs had a ~9-fold increase in their rates of proliferation, identified by EdU incorporation and co-localization with the oligodendrocyte lineage marker Olig2 (Fig. 1g-h). The transient over-expression of *Myc* led to a moderate increase of endogenous *c-Myc* mRNA level 5 days after transfection, the timepoint at which we performed the EdU incorporation assay (Extended Data Fig. 1g).

Since c-Myc is a well characterised oncogene and its expression has been shown to decrease when OPCs differentiate into oligodendrocytes during development [11], as well as during differentiation in our culture system (Extended Data Fig. 1h), we next asked whether the cells retained their differentiation capacity and were not undergoing increased proliferation due to induced transformation. First, we confirmed that aged OPCs retained their cell identity after *c-Myc* over-expression by staining for the oligodendrocyte lineage markers Olig2 and SOX10 as well as for the OPC marker NG2 (Extended Data Fig. 1i). We then tested the ability of aged OPCs after *c-MYC* overexpression to differentiate into oligodendrocytes. To do this, aged OPCs were transfected with *GFP* or *c-Myc* mRNA, cultured for 5 days in proliferation medium and then placed into differentiation condition media containing the pro-differentiation signal T3 for 5 days. Aged OPCs transfected with *GFP* had low rates of differentiation (≤5%), while those transfected with *c-Myc* efficiently differentiated into oligodendrocytes as defined by their co-expression of Olig2 and myelin basic protein (MBP) (Fig. 1g, i). Thus, overexpression of *c-Myc* not only increased aged OPC proliferation, but also their differentiation into oligodendrocytes.

Since c-Myc is sufficient to promote both the proliferation and differentiation of aged OPCs *in vitro,* we hypothesised that its inhibition would lead to a spontaneous aged-like phenotype

in neonatal OPCs (Fig. 2a). The low molecular weight compound 10058-F4 (Myci) inhibits both c-Myc and n-Myc activity by blocking the dimerization of Myc and Max in a reversible manner [12], making it an ideal small molecule for studying the role of *c-Myc* in neonatal OPCs. Previous work found that ES cells treated with Myci remain pluripotent but become dormant, losing proliferative and differentiation capacity: upon restoration of Myc activity, however, ES cells re-enter the cell cycle [13]. To test whether Myc modulation with Myci similarly affects the activity of neonatal OPCs, we first established the maximum non-lethal dose of the compound (Extended Data Fig. 2a-b). We found that 1-16μM Myci resulted in minimal cell death after culturing neonatal OPCs for 48 hours in growth factors. At 16μM after 5 days culturing *in vitro* with the growth factors Fgf and Pdgf-AA, neonatal OPCs lost nearly all of their proliferative capacity, while neonatal OPCs cultured in DMSO maintained their self-renewal capacity as shown by EdU incorporation (Fig. 2b-d). If cells were exiting the cell cycle following inhibition of Myc, then it is possible that the cells were simply differentiating into post-mitotic oligodendrocytes, rather than transitioning to a slowly-cycling adult OPC state. To test for this, we examined the expression of the OPC specific marker A2B5 and the oligodendrocyte specific marker MBP. OPCs treated with Myci continued to express A2B5 but did not increase MBP expression, indicating that they were still in a progenitor state (Fig. 2e).

An alternative explanation would be that the neonatal OPCs treated with Myci, like ESCs, exit the cell cycle but retain the same potential to differentiate, as dormant stem cell populations would do in G0 of the cell cycle. If this were the case, then withdrawing Myci and placing them into differentiation conditions with T3 would result in equally efficient differentiation into MBP expressing oligodendrocytes. Such an outcome would suggest that the OPCs were quiescent rather than aged. To test this, neonatal OPCs were either pre-treated with Myci prior to differentiation or treated with Myci during differentiation (Fig. 2f). Neonatal OPCs placed in differentiation conditions for 5 days following 2 days treatment with 16μM Myci in maintenance conditions continued to express Olig2 but failed to form MBP expressing oligodendrocytes. Conversely, control DMSO-treated cultures maintained their differentiation capacity (Fig. 2g-h). Neonatal OPCs treated with Myci in differentiation conditions also failed to differentiate into MBP expressing oligodendrocytes (Fig. 2g-h). These results show that Myci treatment does not drive terminal differentiation into oligodendrocytes or Olig2 negative astrocytes: rather, inhibition of Myc converts a neonatal

OPC into a deeply quiescent, aged-like OPC that fails to differentiate, even in the absence of Myci.

To address the possibility that these results might be due to off-target effects of F10058-4, we used a genetic approach to interfere with c-MYC in neonatal cells. For this purpose, we transfected Cas9-mRNA and two guide RNAs (gRNAs) targeting *c-MYC* and repeated our experiments assessing proliferation and differentiation (Extended Data Fig. 2c). We confirmed that the transfected OPCs had no significant indel formation at predicted off-target sites (Extended Data Fig. 2d). OPCs transfected with *c-Myc* targeting gRNAs retained their progenitor state, judged by the continued expression of A2B5 and the lack of expression of MBP (Extended Data Fig. 2e). Further gRNAs targeting *c-MYC* led to a knockdown of *c-MYC* mRNA levels (Extended Data Fig. 2f). Like OPCs treated with Myci, OPCs after knockdown of *c-Myc* proliferated and differentiated significantly less (Fig. 2i-k).

We then asked if the state induced by the loss of MYC activity was reversible to distinguish whether the treatment with the inhibitor caused a deep quiescent state, or led to an irreversible cell cycle arrest and loss of differentiation capacity. For this purpose, we cultured neonatal OPCs for 48h in the presence of 16µM Myci, then washed out the inhibitor and assessed the capacity for proliferation and differentiation after 7 or 10 days respectively (Extended Data Fig. 2g). We found that neonatal OPCs initially treated with Myci re-entered the cell cycle and proliferated at levels indistinguishable from control cells that were cultured in medium containing DMSO (Extended Data Fig. 2g, h). More than 30% of OPCs differentiated into MBP positive oligodendrocyte after 10 days after removal of the inhibitor from the culture medium (Extended Data Fig. 2 g,i). Thus, reduced expression or the pharmacological inhibition of MYC induces a deeply quiescent state in neonatal OPCs that functionally mimics an aged OPC state but does not diminish their functional potential.

Myc induces a neonatal like genetic program

If c-Myc activity alone describes the age state of an OPC, we hypothesized that the modulation of c-Myc activity would affect age-related pathways. To test this, we sequenced acutely isolated neonatal and aged OPCs, neonatal OPCs treated with Myci, and aged OPCs transfected with *c-Myc* (Fig. 3a). We found that aged and neonatal OPCs clustered separately,

as shown by hierarchical clustering and principal component analysis (Fig. 3b and Extended Data 3a). Neonatal OPCs that were treated with Myci clustered more closely to acutely isolated aged OPCs, but that these two groups were distinct from all other groups. Aged OPCs transfected with *c-Myc* mRNA clustered more closely with acutely isolated neonatal OPCs than did aged OPCs transfected with *GFP* mRNA.

To better understand the process by which c-Myc modulates the functional capacity of OPCs, we performed gene set enrichment analysis (GSEA) on the transcriptomic data. First, we compared freshly isolated neonatal and aged cells with each other to identify the pathways and biological processes that define the respective age states of OPCs (Fig. 3c, Supplementary Information Table 1). As we have shown previously, there was an enrichment for gene sets involved with metabolism (oxidative phosphorylation), cell cycle, ribosome biogenesis and DNA repair (FDR < 0.05). Aged cells showed an enrichment for focal adhesions, ECM receptor signaling and TGF-beta signaling. When we compared the cells treated *in vitro*, neonatal derived cells exposed to DMSO and aged cells transfected with *c-Myc* showed a similar enrichment for the pathways and processes identified in freshly isolated neonatal cells (Fig. 3d,e). Among all "neonate like" OPCs there was an enrichment of 188 pathways and processes (Fig. 3d) that involved functions such as DNA repair, genomic stability, cell cycle activity, proteostasis, metabolism and intercellular signaling pathways such as WNT signaling (Fig. 3e), all of which are hallmarks of young adult stem cells or implicated in tissue regeneration. Conversely, aged cells transfected with *GFP* or neonatal cells treated with Myci showed an enrichment mainly for inflammatory pathways, which are closely linked to ageing (Extended Data Fig. 3b,c). The convergent enrichment for these specific gene sets emphasizes the importance of *c-Myc* activity on overall cell activity and functional potential.

To establish a link between the levels or the activity of c-Myc and the functional state we examined the DNA damage response, a crucial pathway for the function of adult stem cells. Aged OPCs transfected with *c-Myc* and neonatal OPCs treated with DMSO had an increase in expression of a large number of DNA repair genes, such as the *Ercc1* and *Rad50/51* (Extended Data Fig. 3d,e), which was also reflected in comparative pathway analyses (Fig. 3e,f). To determine the DNA integrity and ability to repair DNA damage following c-Myc activity modulation, we performed a comet assay under alkaline conditions, a technique developed

to detect all forms of DNA damage. Neonatal OPCs *in vitro* treated with DMSO, retained their DNA integrity, with only ~15% of OPCs having DNA damage, as indicated by the proportion of tailed 'comets'. Conversely, in aged OPCs transfected with only *GFP*, ~60% of all OPCs had DNA damage (Fig. 3g,h). We excluded that this difference in DNA damage was due to decreased viability of aged cells at this time point of *in vitro* culture (Extended Data Fig. 3f). Only 30% of comets of aged OPCs transfected with Myc had tailed comets, indicating that DNA damage was reduced by 50% following *c-Myc* transfection. Neonatal OPCs treated with Myci retained their DNA integrity, as indicated by a low proportion of tailed comets, most likely because 5 days *in vitro* is insufficient time to cause high levels of DNA damage, while the low cellular activity of Myci treated cells also spared the cells from DNA damage caused by high metabolic activity. Hence, we decided to test if MYCi treatment reduces the ability of OPCs for DNA repair by inducing DNA damage after MYCi treatment using etoposide, a topoisomerase inhibitor previously identified to induce DNA damage[14]. We identified a concentration of etoposide that was able to induce robust DNA damage while not reducing cell viability significantly (Extended data 4a-d). We found that OPCs pre-treated with MYCi showed a reduced capacity to repair etoposide-induced DNA damage 48h after exposure compared to OPCs pretreated with DMSO, suggesting that a loss of cellular activity by inhibition of MYC significantly impairs the ability of OPCs for DNA repair (Extended data 4e-h). Together, these results indicate that c-Myc activity alone can modulate the genetic stability of aged OPCs, thereby contributing to a neonate-like cell behaviour.

c-Myc is involved in OPC activation during remyelination and rejuvenation

Following demyelination and in the initial stages of remyelination, adult OPCs revert to a more immature state [15] that resembles that of neonatal OPCs treated *in vitro* with DMSO, and aged OPCs transfected with *c-Myc*: for example, both involve increased expression of specific OPC activation genes such as *Sox2* and *Nkx2.2* (Extended Data Fig. 3d). Further, inhibition of Myc activity using Myci reduced the expression of these genes (Extended Data Fig. 3e). We therefore asked whether the transcriptomic changes that occur in adult OPCs at the onset of remyelination are comparable to the changes we have seen after the overexpression of *c-Myc* in aged cells. We used microarray data from a previously published study [15], compared the gene expression of resting adult OPCs and OPCs after induction of a demyelinating lesion and identified enriched pathways in the activated OPCs (Extended Data Fig. 5a). When

compared to the pathways enriched in neonatal OPCs and aged OPCs transfected with *c-Myc*, there was again an overlap of pathways and processes centered around mRNA metabolism, proteostasis, DNA repair, TCA cycle activity, metabolism and proliferation, reflecting the active state of these cells (Extended Data Fig. 5b). These data highlight that Myc overexpression in aged cells can mimic pathway alterations that occur when adult quiescent OPCs become activated during remyelination.

To elucidate which transcription factors control these changes in gene expression we identified enriched motifs of transcription factor binding in the regulatory sequences of the genes higher expressed in activated OPCs. Among these, we found that there was a significant enrichment for the known binding motif of c-Myc, suggesting that the activation of OPCs during remyelination may be at least in part driven by c-Myc (Extended Data Fig. 5c).

We have recently shown that aged OPCs can be converted into an active neonatal-like state when placed on a substrate that mimicked the physical stiffness of a neonate brain [5]. Using the transcriptome generated in our previous study, we again performed a pathway enrichment analysis. Under conditions that allowed OPCs to efficiently proliferate and differentiate, they showed an enrichment of core pathways like TCA cycle, OXPHOS, DNA repair pathways, proteostasis and cell cycle regulation (Extended Data Fig. 5d,e).

By comparing our transcriptomic data to the physiological activation of resting adult OPCs and the functional rejuvenation of aged OPCs on soft substrates, we concluded that an active, functional state of OPCs is characterized by gene networks that can be activated by overexpression of *c-Myc*. These gene networks, as expected, include pathways related to cell cycle control. However, our data also underlines the role of c-Myc in the general regulation of cellular metabolism, DNA repair and proteostasis, all processes which are linked to activated and young stem cells.

Re-activation of aged OPCs by over-expression of *c-Myc* enhances myelin regeneration *in vivo*

We next asked whether the re-activation of aged OPCs by increased c-Myc activity could improve myelin regeneration in the aged CNS. To address this, we repurposed recently

developed molecular biology tools. Using a novel, synthetically created, and systemically administered AAV (PHP-EB), we reasoned that it would be possible to target large numbers of OPCs in the CNS [16]. In conjunction with the AAV, we used a recently developed CRISPR technique which allows for the sequence-specific integration of genomic fragments into slowly-dividing/post-mitotic cells [17]. With these two technologies, we developed a dual AAV system, that we had used previously to genetically engineer aged OPCs *in vivo* [5]: one virus delivers the spCas9 gene controlled by the CMV promoter, while the other delivers a construct which contains both an overexpression sequence for 3'UTR-targetting Pdgfra gRNA and a knock-in vector containing IRES-*GFP-T2A-Myc*, flanked by reversed gRNA target sequences (Fig. 4a, Extended Data Fig. 5a). This system allows for *GFP* and *Myc* to be expressed in all *Pdgfra* expressing OPCs of the CNS following a single intravenous injection of the dual-AAV system. Moreover, by integrating the fragment into the 3' UTR, we avoided perturbing the gene expression of *Pdgfra* itself. Thus, this approach allowed for the controlled, OPC-restricted expression of *c-Myc*: once the OPC differentiates into an oligodendrocyte and downregulates *Pdgfra*, *c-Myc* expression is also lost.

To confirm that this CRISPR AAV system works, we infected cells isolated from neonatal mouse CNS with the vectors. As a mixed cell population, GFP should only be expressed in cells also expressing the oligodendroglia lineage marker Olig2. Five days following infection, we found Olig2 expressing cells also expressing GFP, but no GFP expression in Olig2 negative cells (Extended Data Fig. 6b). We further confirmed the successful translation of the proteins encoded in the viruses by Western Blot after transducing neonatal mouse OPCs *in vitro* (Extended Data Fig. 6c, Supplementary Information Figure 1). We next tail-vein-injected both AAVs into aged 18-month-old mice, and two weeks later induced a focal area of demyelination in the spinal cord white matter by the injection of lysolecithin. Lesioned mice were then perfused after a further 2 weeks, when remyelination is ongoing and thus changes in rate can be detected (Fig. 4b). Four weeks following the initial tail vein injection, DNA PCR on the DNA of isolated OPCs from cerebral cortex revealed the correct genomic integration of the control, GFP-only vector and of the GFP-c-Myc vector (Extended Data Fig. 6d). Cryo-sections of un-lesioned grey and white matter in the spinal cord showed over 35% of Olig2 expressing cells staining positive for GFP and <10% of total GFP cells were negative for Olig2 (Extended Data Fig. 6e-f), confirming that the CRISPR knock-in efficiently targets the CNS and

that the expression locus is highly specific for oligodendrocyte lineage cells. The identity of all the GFP expressing cells that were not Olig2 positive is unclear - very few of these expressed markers for pericytes, astrocytes or microglia (Extended Data Fig. 6g-j). qPCR on the RNA from isolated aged OPCs revealed a 4-fold upregulation of *c-Myc* transcript in the animals that received the c-Myc-GFP AAV compared to animals that received the GFP only vector (Fig. 4c). To determine the rate of OPC proliferation in c-Myc-AAV infected animals, EdU was administered by intraperitoneal injection 24 hours prior to perfusion fixation. In homeostatic grey and white matter, there were no significant changes in the rate of OPC proliferation. Within the lesion of the control GFP-infected animal, EdU labelled approximately 10% of the Olig2 stained cells (Fig. 4d,e; Extended Data Fig. 6k). In the c-Myc vector-infected animals, however, ~40% of the Olig2 stained cells in the lesion were labelled with EdU. Among, these EdU positive cells in c-Myc infected animals were in the majority GFP positive cells. In the control GFP infected animals, there were few Olig2+, CC1+ oligodendrocytes, whereas in the c-Myc infected animals, there was an almost 4-fold increase in the number of labeled CC1+ and Olig2+ oligodendrocytes within the lesion (Fig. 4f,g). We quantified the effects on proliferation and differentiation among all Olig2+ cells instead of the GFP positive subpopulation because of the dependency of the GFP signal on the expression of PDGFRA. Upon initiation of differentiation, OPCs stop expressing PDGFRA with the consequence that GFP negative cells can be cells that recently started to differentiate or cells that did not carry the introduced expression cassette. When analysing the GFP subpopulation, we found that GFP+ Olig2+ cells incorporated EdU at a higher frequency compared to GFP- Olig2+ in c-MYC infected animals, confirming that MYC overexpression improved the function of aged OPCs (Extended Data Fig.6l). However, the proportion of GFP-/Olig2+ EdU+ cells was significantly higher compared to Olig2 positive cells from control transfected animals, suggesting that c-MYC overexpressing cells could have, directly or indirectly, improved the function of adjacent OPCs. However, it is also possible that GFP negative cells resemble a population of OPCs that initiated differentiation after a final round of cell division, which would have led to the loss of the PDGFRA dependent expression of the GFP marker.

To address if the enhanced function of aged OPCs in c-Myc AAV infected animals also translated into a better regenerative outcome, we infected aged animals again with viruses

encoding for *GFP* or *c-Myc-GFP* and assessed remyelination in ultra-thin resin sections using electron microscopy 28 days post lesion. We quantified the extent of remyelination as the percentage of remyelinated axons [4,5]. As expected, GFP infected aged animals showed poor remyelination, while in c-Myc infected animals the extent of remyelination was consistently higher (Fig. 4 h-j).

Together, these results reveal that 1) c-Myc not only causes the proliferation of aged OPCs into the lesion area, but also their differentiation into oligodendrocytes, 2) the controlled-expression of *c-Myc* can functionally rejuvenate aged OPCs within the context of myelin regeneration, 3) and the functional rejuvenation of aged OPCs on their own can accelerate remyelination in aged animals (Fig. 4k).

DISCUSSION

Cellular activity determines the regenerative capacity of a progenitor/stem cell

In this study we explore which of the pluripotency-inducing transcription factors are needed to induce age-reversal through partial reprograming. We find that overexpression of *c-Myc* alone is sufficient to convert aged dysfunctional OPCs into highly functional neonate-like cells *in vitro* (Fig. 1). Using a recently developed strategy for genetic engineering *in vivo* [5], we were also able to enhance the capacity of aged OPCs to proliferate and differentiate *in vivo* and thereby improve remyelination in aged animals in which the natural tempo of remyelination is profoundly limited (Fig. 4). This enhancement in regeneration is a surprising finding since young OPCs, like young muscle stem cells, lose their youthful phenotype and regenerative capacity after transplantation into an aged environment [5,18]. Our data suggest that it is neither the chronological nor biological age of the cell that determines the regenerative potential, but its functional state. In support of this idea, we recently demonstrated that the deletion of *Piezo1*, a mechano-sensing channel, was sufficient to convert dysfunctional aged OPCs into cells with a functional potential of neonatal OPCs in an aged environment. Moreover, inhibiting *Piezo1* expression in neonatal OPCs, protected them from a functional decline when transplanted into an aged brain [5]. Similarly, re-activation of aged quiescent muscle stem cells *in vitro* using biochemical and biophysical interventions before the

transplantation into aged muscle preserved their rejuvenated state *in vivo* [18]. These data suggest that once a stem cell initiates an endogenous activity program, the capacity to undergo proliferation and differentiation remain largely cell-autonomous. However, the possibility exists that stem cells, in which such an activation program has been initiated, provide signals that improve the function of cells in their vicinity, which could then iteratively influence the function of the stem cells themselves. In line with this, we found that the GFP positive cells proliferated to a higher extent than aged OPCs in lesions of control transfected animals (Extended Data Fig. 6l). Thus, the observed enhancement of the regenerative response in our study could, in part, rely on the creation of an environment that is more permissive for regeneration compared to that in wild type animals, a possibility that our genetic approach does not address.

The concept that the stem cell program after activation is largely a cell-autonomous process is consistent with observations made in aged neural stem cells, which exhibit the same functional capacity as young neural stem cells once they are activated [19]. Indeed, activated neural stem cells, regardless of their chronological age, have a transcriptome more similar to each other than to their quiescent age-matched controls. These data suggest that while the regenerative potential of adult stem cells is only partially dependent on their environment, their ability to become activated is environment-dependent. In this regard, alterations that occur in the niche with ageing enforce an inactive state in adult stem cells. For example, neural stem cells lose their proliferative capacity in response to inflammatory signals [19], as do OPCs in response to niche stiffening [5]. Hence, interventions that mitigate the age-related changes of the niche are currently seen as promising strategies to re-activate aged stem cells for regeneration. Our data show that it is also possible to directly activate genetic networks within aged stem cells that lead to their activation, and the activity state of a stem cell masks the chronological age of that cell.

c-Myc drives biological processes that lead to progenitor/stem cell activation and rejuvenation

The role of c-Myc in the proliferation and differentiation of stem cells and how these cells interact with their niche has been widely explored, especially in the hematopoietic system [19]. For example, loss of c-Myc in bone marrow leads to an expansion of HSCs due to a failure of

these stem cells to activate, leave their niche and undergo differentiation [20]. We found that overexpression of *c-Myc* leads to the increased expression of genes that are associated with a higher metabolic rate, DNA repair mechanisms and ribosome biogenesis, all of which are cellular processes characteristic of young, rejuvenated and active adult stem cells. The stimulation of these processes can achieve both the activation of a quiescent stem cell and the functional rejuvenation of an aged stem cell. An example of this is the modulation of cellular metabolism: the activation of muscle, neural and hematopoietic stem cells depends on the increase of metabolic function [21]. At the same time, interventions like fasting or calorie-restriction mimetics like metformin, which target crucial nutrient signalling pathways, primarily lead to an increase in metabolic function, thereby re-activating aged stem cells for repair [4,22,23]. We have also shown that the overexpression of *c-Myc* improves DNA repair in aged OPCs, which was also a feature of OPCs rejuvenated by fasting, metformin or exposure to a soft environment [4,5]. Likewise, hematopoietic stem cells engage in DNA repair when they are activated [24].

In contrast, if highly active stem cells such as neonatal OPCs, intestinal stem cells or mouse embryonic stem cells are forced into quiescence, they decrease expression of genes associated with DNA repair, cellular metabolism and protein biosynthesis [13,25]. These data indicate that rejuvenating treatments and the natural activation of stem cells use similar molecular programmes to achieve a highly regenerative state to those involved in ageing and quiescence. The molecular programmes driving cell activation or quiescence can be controlled via the modulation of c-Myc activity. c-Myc is not only associated with the activation of the gene network characteristic of activated OPCs but also with that of neural stem cells [26], and loss of c-Myc function in hematopoietic stem cells leads to the loss of the activated HSC compartment and all of its progeny [27].

The governing forces that determine c-Myc activity and its declining expression with age remain unclear. There is some evidence that c-Myc activity is determined by cellular exposure to exogenous platelet derived growth factor (PDGF) [28]. OPC activity has been concretely linked to PDGF exposure in the adult CNS [29]. Despite this, as documented in this work, high *in vitro* concentrations of PDGF are insufficient to re-activate aged OPCs, indicating additional

regulatory networks are involved in determining c-Myc activity in aged cells. Likely, there are a number of intersecting mechanisms that govern c-Myc activity in adult stem cells, including exposure to growth factors, niche matrix components, cell density, and intrinsic cell-cycle checkpoints that limit uncontrolled cellular growth [30]. Future work will be to unravel these precise mechanisms that govern c-Myc activity in development and limit its expression in the aged CNS.

The therapeutic potential of progenitor/stem cell activation

Does this mean an active state prevents ageing? Different adult stem cell populations throughout the body follow different dynamics to ensure tissue homeostasis. This difference reflects the demand for cell replacement which is inherently low for long-lived cells like oligodendrocytes in the brain but which is high for the blood or gut system. Compared to the stem cell systems with slower turnover, the ageing of more active hematopoietic and intestinal stem cells is not characterised by a marked loss of the capacity to proliferate and differentiate. At the same time, enforcing the activity of stem cell pools with a slower turnover could bring new problems, such as stem cell exhaustion and a higher incidence of cancer cells. A recent study using skin stem cells revealed that stem cells during development and regeneration shared a molecular program of cell activity and growth with cancer-initiating cells [31]. However, the study of continuously active stem cell compartments might also shed light on how to fine-tune the activation of quiescent adult stem cells for repair, while minimising the chance of exhaustion or oncogenic transformation. Finally, the therapeutic potential of an intervention that aims to promote the activation of stem cells alone will not be as powerful as treatments that lead to an overall rejuvenation effect of the stem cells and their environment such as fasting or the treatment with metformin [4,22]. Some components of the regenerative process such as the myelination of an axon, might be independent of the stem cell program can be effectively stalled by a lesion environment replete with inhibitors of differentiation such as myelin debris [32].

In summary, our results demonstrate that the manipulation of c-Myc alone is sufficient to reset the functional age of OPCs, irrespective of their chronological age. The pathways which we found to be enriched for in rejuvenated or neonatal cells are classically associated with the activation of adult stem cells, such as oxidative phosphorylation, DNA repair, and

ribosome biogenesis. In light of this, our data suggest that the activity state of a stem cell reflects its functional age. Consequently, understanding the genetic pathways that lead to the activation of adult stem cells may hold great therapeutic potential for regenerative medicine.

Acknowledgments

This work was supported by funding from the UK Multiple Sclerosis Society (MS50), MedImmune, The Adelson Medical Research Foundation and a core support grant from the Wellcome Trust and MRC to the Wellcome Trust-Medical Research Council Cambridge Stem Cell Institute (203151/Z/16/Z).

Author Contributions

Conceptualization, B.N., M.S., and R.J.M.F.; Methodology, M.S. and B.N..; Investigation, M.S., B.N., C.Z., P.T, A.Y., S.F. and A.S.; Formal Analysis, M.S., B.N., C.Z., K.R., K.C. and R.J.F.M.; Writing B.N., M.S., K.C. and R.J.M.F.; Microarray analysis, T.G.; Funding Acquisition R.J.M.F., Supervision K.C. and R.J.M.F.

Competing interests statement

The authors declare that there are no competing interests.

REFERENCES

1. Zawadzka, M. *et al.* CNS-resident glial progenitor/stem cells produce Schwann cells as well as oligodendrocytes during repair of CNS demyelination. *Cell Stem Cell* **6,** 578–590 (2010).
2. Hill, R. A., Li, A. M. & Grutzendler, J. Lifelong cortical myelin plasticity and age-related degeneration in the live mammalian brain. *Nat. Neurosci.* **26,** R971 (2018).
3. Young, K. M. *et al.* Oligodendrocyte dynamics in the healthy adult CNS: evidence for myelin remodeling. *Neuron* **77,** 873–885 (2013).
4. Neumann, B. *et al.* Metformin Restores CNS Remyelination Capacity by Rejuvenating Aged Stem Cells. *Cell Stem Cell* **25,** 473–485.e8 (2019).
5. Segel, M. *et al.* Niche stiffness underlies the ageing of central nervous system progenitor cells. *Nature* **350,** 1199–5 (2019).
6. Sim, F. J., Zhao, C., Penderis, J. & Franklin, R. J. M. The age-related decrease in CNS remyelination efficiency is attributable to an impairment of both oligodendrocyte progenitor recruitment and differentiation. *J. Neurosci.* **22,** 2451–2459 (2002).
7. Lapasset, L. *et al.* Rejuvenating senescent and centenarian human cells by reprogramming through the pluripotent state. *Genes Dev.* **25,** 2248–2253 (2011).
8. Ocampo, A. *et al.* In Vivo Amelioration of Age-Associated Hallmarks by Partial Reprogramming. *Cell* **167,** 1719–1733.e12 (2016).
9. Sarkar, T. J. *et al.* Transient non-integrative expression of nuclear reprogramming factors promotes multifaceted amelioration of aging in human cells. *Nat. Commun.* **11,** 1545–12 (2020).
10. Tabula Muris Consortium. A single-cell transcriptomic atlas characterizes ageing tissues in the mouse. *Nature* **583,** 590–595 (2020).
11. Magri, L. *et al.* c-Myc-dependent transcriptional regulation of cell cycle and nucleosomal histones during oligodendrocyte differentiation. *Neuroscience* **276,** 72–86 (2014).
12. Zirath, H. *et al.* MYC inhibition induces metabolic changes leading to accumulation of lipid droplets in tumor cells. *Proc. Natl. Acad. Sci. U.S.A.* **110,** 10258–10263 (2013).
13. Scognamiglio, R. *et al.* Myc Depletion Induces a Pluripotent Dormant State Mimicking Diapause. *Cell* **164,** 668–680 (2016).
14. Tamamori-Adachi, M. *et al.* DNA damage response induced by Etoposide promotes steroidogenesis via GADD45A in cultured adrenal cells. *Sci Rep* **8,** 9636–13 (2018).
15. Moyon, S. *et al.* Demyelination causes adult CNS progenitors to revert to an immature state and express immune cues that support their migration. *J. Neurosci.* **35,** 4–20 (2015).
16. Challis, R. C. *et al.* Systemic AAV vectors for widespread and targeted gene delivery in rodents. *Nat. Protoc.* **14,** 379–414 (2019).
17. Suzuki, K. *et al.* In vivo genome editing via CRISPR/Cas9 mediated homology-independent targeted integration. *Nature* **540,** 144–149 (2016).
18. Cosgrove, B. D. *et al.* Rejuvenation of the muscle stem cell population restores strength to injured aged muscles. *Nat. Med.* **20,** 255–264 (2014).
19. Kalamakis, G. *et al.* Quiescence Modulates Stem Cell Maintenance and Regenerative Capacity in the Aging Brain. *Cell* **176,** 1407–1419.e14 (2019).
20. Wilson, A. *et al.* c-Myc controls the balance between hematopoietic stem cell self-renewal and differentiation. *Genes Dev.* **18,** 2747–2763 (2004).
21. Ryall, J. G., Cliff, T., Dalton, S. & Sartorelli, V. Metabolic Reprogramming of Stem Cell Epigenetics. *Cell Stem Cell* **17,** 651–662 (2015).
22. Cerletti, M., Jang, Y. C., Finley, L. W. S., Haigis, M. C. & Wagers, A. J. Short-term calorie restriction enhances skeletal muscle stem cell function. *Cell Stem Cell* **10,** 515–519 (2012).
23. Mihaylova, M. M., Sabatini, D. M. & Yilmaz, O. H. Dietary and metabolic control of stem cell function in physiology and cancer. *Cell Stem Cell* **14,** 292–305 (2014).

24. Beerman, I., Seita, J., Inlay, M. A., Weissman, I. L. & Rossi, D. J. Quiescent hematopoietic stem cells accumulate DNA damage during aging that is repaired upon entry into cell cycle. *Cell Stem Cell* **15,** 37–50 (2014).
25. Basak, O. *et al.* Induced Quiescence of Lgr5+ Stem Cells in Intestinal Organoids Enables Differentiation of Hormone-Producing Enteroendocrine Cells. *Cell Stem Cell* **20,** 177–190.e4 (2017).
26. Leeman, D. S. *et al.* Lysosome activation clears aggregates and enhances quiescent neural stem cell activation during aging. *Science* **359,** 1277–1283 (2018).
27. Laurenti, E. *et al.* Hematopoietic stem cell function and survival depend on c-Myc and N-Myc activity. *Cell Stem Cell* **3,** 611–624 (2008).
28. Chiariello, M., Marinissen, M. J. & Gutkind, J. S. Regulation of c-myc expression by PDGF through Rho GTPases. *Nat. Cell Biol.* **3,** 580–586 (2001).
29. Woodruff, R. H., Fruttiger, M., Richardson, W. D. & Franklin, R. J. M. Platelet-derived growth factor regulates oligodendrocyte progenitor numbers in adult CNS and their response following CNS demyelination. *Mol. Cell. Neurosci.* **25,** 252–262 (2004).
30. Vervoorts, J., Lüscher-Firzlaff, J. & Lüscher, B. The ins and outs of MYC regulation by posttranslational mechanisms. *J. Biol. Chem.* **281,** 34725–34729 (2006).
31. Ge, Y. *et al.* Stem Cell Lineage Infidelity Drives Wound Repair and Cancer. *Cell* **169,** 636–650.e14 (2017).
32. Kotter, M. R., Li, W.-W., Zhao, C. & Franklin, R. J. M. Myelin impairs CNS remyelination by inhibiting oligodendrocyte precursor cell differentiation. *J. Neurosci.* **26,** 328–332 (2006).
33. McMurran, C. E., Zhao, C. & Franklin, R. J. M. Toxin-Based Models to Investigate Demyelination and Remyelination. *Methods Mol. Biol.* **1936,** 377–396 (2019).
34. Schindelin, J. *et al.* Fiji: an open-source platform for biological-image analysis. *Nat. Methods* **9,** 676–682 (2012).
35. Olive, P. L. & Banáth, J. P. The comet assay: a method to measure DNA damage in individual cells. *Nat Protoc* **1,** 23–29 (2006).
36. Collins, A. R. The comet assay for DNA damage and repair: principles, applications, and limitations. *Mol. Biotechnol.* **26,** 249–261 (2004).
37. Ho, J. W. K., Stefani, M., Remedios, dos, C. G. & Charleston, M. A. Differential variability analysis of gene expression and its application to human diseases. *Bioinformatics* **24,** i390–8 (2008).
38. Ritchie, M. E. *et al.* limma powers differential expression analyses for RNA-sequencing and microarray studies. *Nucleic Acids Res.* **43,** e47–e47 (2015).
39. Heinz, S. *et al.* Simple combinations of lineage-determining transcription factors prime cis-regulatory elements required for macrophage and B cell identities. *Mol. Cell* **38,** 576–589 (2010).

FIGURE LEGENDS

Fig. 1. *c-MYC* overexpression reactivates aged OPCs. **(a),** Diagram illustrating the underlying principle of partial reprogramming for rejuvenating aged OPCs. **(b),** Representative images of EdU incorporation and MBP expression in Olig2 stained aged OPCs transfected with either *GFP* or *c-Myc* modified mRNA. **(c-d)** Quantification of the data for EdU incorporation and MBP expression, respectively (N=3-4 biological repeats for each group), **(e)** Schematic overview of *in vitro* gene screening assay for aged OPC activation. **(f),** A heatmap of the log2 transformed FPKM values from RNAseq of the pluripotency factors *Oct4*, *Sox2*, *Klf4*, and *c-Myc* in neonatal versus aged rat OPCs. **(g),** Representative images of EdU incorporation and MBP expression in Olig2 stained aged OPCs transfected with either *GFP* or *c-Myc* modified mRNA. **(h,i)** Quantification of the data for EdU incorporation and MBP expression, respectively. Bar charts represent mean from N=3 biological replicates and error bars represent standard deviation. Scale bars represent 50μm. Statistical significance was determined using two-tailed t-tests.

Fig. 2. Inhibition of Myc induces an aged-like phenotype in neonatal OPCs. **(a),** Schematic outlining experimental strategy for Myci treatment of neonatal OPCs. **(b,c),** Representative images and quantifications of EdU incorporation from N=3 biological replicates showing the effects of varying concentrations of Myci on Olig2+ neonatal OPCs. **(c),** Quantification of EdU incorporation after Myci treatment. **(d),** Higher magnification images of EdU incorporation of neonatal OPCs treated with DMSO or Myci. **(e),** Representative image demonstrating that Myci treated OPCs remain OPCs and do not differentiate after cell cycle exit. **(f)** Schematic outlining strategy for understanding the effects of Myci on neonatal OPC differentiation. **(g-h),** Representative images and quantifications of the effects of Myci on the differentiation of Olig2+ neonatal OPCs into MBP+ oligodendrocytes. OPCs were either treated with Myci in proliferation conditions (P) or in differentiation conditions (D). **(i),** Representative images of neonatal OPCs after transfection with spCas9 and Myc targeting gRNAs to assess their proliferation (EdU incorporation) or differentiation (MBP expression) ability. **(j-k),** Quantification of EdU incorporation and differentiation into oligodendrocytes (MBP+/Olig2+) N=3 biological repeats for each group. Scale bars represent 50μm. Statistical significance was determined using One-Way ANOVA and Tukey's multiple comparisons test.

Fig. 3. Transcriptomic modulation of OPC age state with c-Myc activity. (a), Schematic outlining the RNAseq strategy and sample collection. Samples reflecting actively cycling and differentiating cells are labelled 'neonate like OPCs'. OPCs that fail to proliferate and differentiate are labelled as 'aged like OPCs'. **(b),** Hierarchical clustering with Ward linkage of acutely isolated aged OPCs, neonatal OPCs, aged OPCs transfected *in vitro* with *c-Myc* or *GFP*, and neonatal OPCs treated with Myci or with DMSO. **(c),** Volcano plot of pathways and biological processes identified after Gene set enrichment analysis comparing aged (blue) and neonatal OPCs (red). NES: normalised enrichment score. FDR < 0.05 for all pathways considered to be enriched in either of the groups. **(d),** Venn diagram showing the overlap of enriched pathways and processes between neonatal OPCs, aged OPCs transfected with *c-Myc* and neonatal OPCs treated with DMSO. **(e),** NES values are plotted for example processes enriched in all 'neonate like OPCs'. **(f),** Example GSEA plot for the GO Term DNA Repair. **(g),** Representative images and quantifications of the comet assay for DNA damage. **(h),** Quantifications represent the mean for each labelled cell group from N=3 biological replicates. For each replicate 50-100 nuclei were quantified.

Fig. 4. Systemic, cell-type specific, *in vivo* CRISPR knock in of *c-Myc* functionally rejuvenates aged OPCs and enhances remyelination. (a), Schematic outlining the control and Myc overexpressing AAV vectors. **(b),** Schematic overview of *in vivo* CRISPR experiment. **(c),** qPCR for *c-Myc* from N=3 homogenized aged mouse cortex 3 weeks post AAV tail vein injection of either *GFP* or *c-Myc* overexpression vector. ΔΔCT normalised to housekeeping gene Tbp. **(d,e),** Representative images and quantifications of EdU incorporation in GFP/Olig2 stained aged lesion cores. **(f,g),** Representative images and quantifications of CC1/Olig2 co-labelling per mm2 in aged lesion cores. **(h,i),** Representative images of ultrathin resin sections stained with lead acetate to visualise remyelination. **(j),** Quantification of remyelination as the percentage of remyelinated axons (N=4 animals for each group). **(k),** Schematic overviewing the role of c-Myc in determining the age state of OPCs. Means represent averages from N=3 animals (e,g) and N=4 animals (j), scale bars show 50µm in D-E and 5µm in h-i, and * represents a p-value of <.01 using a two tailed t-test. Statistical significance of remyelination determined a two-tailed t-test.

Extended Data Fig. 1. Transfection of Myc but not Sox2 reactivates aged rat OPCs. **(a),** Schematic illustrating the transfection strategy using mRNAs. **(b,c),** Representative images and quantifications of the transfection efficiency of modified mRNA in aged OPCs. Control transfections were transfected with lipofectamine without mRNA encoding *GFP*. Scale bars represent 100µm. **(d),** Scatterplots of scRNAseq data for *c-MYC* expression in *Olig2* and *CSPG4* expressing cells in 3 and 24 month old animals. Data produced from (https://tabula-muris-senis.ds.czbiohub.org). **(e),** qPCR results measuring relative abundance of MYC mRNA in freshly MACs sorted neonatal and aged OPCs. N=3 biological repeats. **(f),** Representative images of EdU incorporation in aged OPCs transfected with *GFP* or *Sox2* (N=2). **(g),** qPCR results measuring relative abundances of *c-Myc* mRNA 5d in aged OPCs after transfection with *GFP* or *c-Myc* mRNA. Means represent averages from N=3 biological replicates. **(h),** qPCR results measuring relative abundances of *c-Myc* mRNA in proliferating or differentiating neonatal OPCs 3 days after culture in the respective culture conditions. (N=3 biological repeats for each group). **(i)**, Representative images of aged OPCs 5 days after transfection with *c-Myc* mRNA stained with the oligodendrocyte lineage markers Olig2, SOX10, and the OPC marker NG2 (n=2 technical replicates). Unless otherwise indicated, scale bars represent 50µm. All bar-graphs represent mean ± SD.

Extended Data Figure 2. CRISPR mediated knockdown of *c-MYC* diminishes the proliferation and differentiation capacity of neonatal OPCs. **(a-b),** Representative images and quantification of live cell stain CalceinAM following neonatal OPC treatment with increasing doses of Myci. **(b),** Quantification of cell viability as the frequency of Calcein AM/DAPI co-positive cells. N=3 biological repeats. **(c),** Schematic illustrating the strategy for the CRISPR experiments. **(d),** off target indel rates, predicted by CRISPOR, quantified by TIDE of the two Myc targeting gRNAs. **(e),** Representative image of neonatal cells 5d stained with the OPC marker A2B5 and the oligodendrocyte marker MBP 5d after transfection with spCas9 and gRNAs. **(f),** qPCR for *c-Myc* in neonatal OPCs after transfection with *Cas9* and control or *c-Myc* targeting gRNAs. **(g),** Representative images of EdU incorporation and MBP expression in Olig2 stained neonatal OPCs treated with either DMSO or MYC-inhibitor for 48h and then cultured without the inhibitor or solvent for an additional 7d or 10d in proliferation or differentiation conditions respectively. **(h,i)**, Quantification of the data for EdU incorporation

and MBP expression, respectively. Scale bars represent 50µm. Means represent N=3 biological replicates ±SD. Statistical significance was determined using two-tailed t-tests.

Extended Data Fig. 3. Inflammatory pathways are enriched in all OPCs with an age-like phenotype. **(a),** Principal component analysis (PCA) of mRNA sequencing of primary aged OPCs, primary neonatal OPCs, *in vitro* aged OPCs, *in vitro* neonatal OPCs, neonatal OPCs treated with Myci, and aged OPCs transfected with modified mRNAs encoding MYC. **(b),** treated Venn diagram illustrating the overlapping pathways and processes in aged OPCs, neonatal OPCs treated with Myci and neonatal OPCs cultured on stiff hydrogels (data from ref 5). **(c),** NES values are plotted for example processes enriched in all 'aged like' OPCs. **(d-e),** Selected genes from various genesets show a number of differentially expressed genes between (d) aged cells transfected with GFP and c-Myc neonatal OPCs or (e) neonatal OPCs treated with DMSO or Myci. **(f),** Quantification of viability assay comparing neonatal and aged OPCs at the time-point of the comet assay in figure 3f. Means represent N=3 biological repeats ±SD.

Extended Data Fig. 4. Increased MYC reduces DNA damage in aged OPCs while MYC inhibition impairs DNA repair in neonatal OPCs. **(a),** Schematic outlining of the experiments. **(b),** Representative images of cells stained with the viability marker Calcein AM. **(c),** Quantification of the total number of cells counted in 9 microscope fields, N=3. **(d),** Quantification of the viability as the frequency of Calcein AM positive cells among all cells, N=3. **(e),** Representative images of comet assays 2h after treatment with DMSO or 1µM Etoposide (ETS), N=2 biological replicates. **(f),** Quantification of the comet assay. **(g),** Representative images of comet assays of cells cultured for 48h in DMSO or MYCi prior to exposure to ETS (2h) and 48 in normal medium. **(h),** Quantification of the comet assay depicted in g. N=2 biological replicates. ETS: Etoposide

Extended Data Fig. 5. All neonate like OPCs share pathways that reflect stem cell activity. **(a),** Venn diagram illustrating the overlapping pathways and processes in neonatal OPCs, aged OPCs transfected with Myc and activated OPCs isolated from the brains of mice 5 weeks after cuprizone treatment (data from ref 15). **(b),** NES values are plotted for example processes

enriched in “neonate like” and activated OPCs. **(c),** Top-5 transcription factors identified by transcription factor binding site analysis using HOMER2. Genes used for analysis were significantly higher expressed in activated versus resting OPCs (log2 fold change >1, adjusted p-value < 0.05, reanalysed data from Moyon et al., 2015). **(d),** Venn diagram illustrating the overlapping pathways and processes in neonatal OPCs, aged OPCs transfected with *c-Myc* and rejuvenated aged OPCs that were cultured on soft hydrogels (data from ref 5). **(e),** NES values are plotted for example processes enriched in “neonate like” and rejuvenated aged OPCs cultured on soft hydrogels.

Extended Data Fig. 6. *In vivo* CRISPR knock-in of *c-Myc* into the 3’UTR of *Pdgfra*. (a), Schematic overview of the predicted knock-in fragments following *in vivo* CRISPR in the 3’UTR of *Pdgfra*. The primers used to identify correct genomic integration 3 weeks following tail vein injection are highlighted as arrows. **(b),** Representative images of mixed glia cultures transduced with AAVs used to achieve the genetic modifications described in a. GFP is only expressed by Olig2 expressing cells. **(c),** Western Blot for GFP and Actin from neonatal mouse OPCs transduced with either the IRES-*GFP* or IRES-*MYC-T2A-GFP* AAVs. (N=2 technical replicates for each experimental group). **(d),** PCR results confirming the integration of viral constructs into the 3’UTR of *Pdgfra*. **(e),** Representative image and of un-lesioned white/grey matter of the spinal cord reveal the efficiency of our *in vivo* CRISPR system and of the expression specificity of Pdgfra for Olig2 expressing OPCs—only ~10% of GFP positive cells are not Olig2+. **(f),** Quantification of transduction efficiency in vivo. **(g-i),** Representative images of spinal cords after transduction with AAVs. Identity of GFP cells was tested for PDGFRB (pericytes), IBA1 (microglia) and GFAP (astrocytes). **(j),** Quantification of the data presented in g-i. N=3 biological replicates. **(k),** Representative images of lesions (below the dotted line) stained for GFP, Olig2 and incorporated EdU 14d post lesion induction. Averages represent mean from N=3 animals and scale bar represents 100µm. **(l),** Quantification of the frequency of GFP positive cells among EdU+Olig2+ cells at 14 dpl.

Supplementary Information Fig. 1. *Full Western Blot images related to Extended Data figure 6c*.

Supplementary Information Table 1. ***Complete results table for GSEA comparing aged and neonatal OPCs in Figure 2c***.

Supplementary Information Table 2. ***Key resources, reagents and oligonucleotide sequences***

METHODS

Lead contact and materials availability

Further information and requests for resources and reagents should be directed to and will be fulfilled by the Lead Contact, Robin Franklin (rjf1000@cam.ac.uk). This study did not generate new unique reagents.

Experimental models and subject details

Animal husbandry

All animal procedures were performed in compliance with United Kingdom Home Office regulations. The animals were housed under standard laboratory conditions on a 12h light/dark cycle with constant access to food and water. All animals were housed in pairs or groups of up to 6 animals. All animals were randomly allocated to experimental groups. All experimental groups were matched for age and gender.

Method details

Induction of white matter lesions and assessment of remyelination

A focal demyelinating spinal cord lesion was induced in 18 months old C57 Black 6 mice [33]. The mice were anesthetized with buprenorphine (0.03mg/kg, s.c.) and 2.5% isoflurane). The spinal cord was exposed between two vertebrae of the thoracic column. Demyelination was induced by injection of 0.8µl of 1% lysolecithin (L-lysophosphatidylcholine, Sigma) into the ventral funiculus at a rate of approximately 1 µl/min. After lysolecithin delivery, the injection needle remained in position for an additional minute.

To assess remyelination the mice were transcardially perfused with 4% glutaraldehyde and 0.4 mM $CaCl_2$ in PBS. The spinal cord was cut into transverse 1mm thick sections. The tissue was fixed in 2% osmium-tetroxide at 4ºC overnight, dehydrated through a series of washes in ethanol and propylene-oxide and embedded in resin. From the resin blocks 1µm thick sections were cut and stained with 1% toluidine blue. Single blocks from each animal from which sections containing the largest area of lesion were identified and used for subsequent

analysis. For electron microscopy (EM), ultrathin sections of lesion sites were cut and transferred onto copper grids. The sections were stained with lead citrate and imaging was performed using a Hitachi-HT7800 Transmission Electron Microscope. In resin sections, remyelinated axons can be readily distinguished from normally myelinated axons outside the lesion by the thinness of the myelin sheath. Within the lesion, remyelinated axons can be distinguished from demyelinated axons because the former have myelin sheaths recognizable as a dark staining rim around the axon. Sections from each animal were examined by an observer blind to the experimental group form which the animal came. For each lesion the proportion of remyelinated axons was determined. For illustration purposes remyelinated and demyelinated axons were pseudo-colored.

Isolation of adult oligodendrocyte progenitor cells

Adult male and female rats (2-24 months) were decapitated after lethal injection with phenobarbital. The brains were removed quickly and placed into ice-cold isolation medium (SI Tab. 1, alternatively Hibernate-A Brainbits). The telencephalon and cerebellum were dissected in isolation medium; meninges, and the olfactory bulb were mechanically removed and the brain tissue was mechanically minced into 1mm^3 pieces. The tissue pieces were spun down at 100g for 1min at RT and the tissue was washed in HBSS- (no Mg2+ and Ca2+, Gibco). Each half of the brain was mixed with 5ml of dissociation solution (34U/ml papain (Worthington), 20µg/ml DNAse Type IV (Gibco) in isolation medium). The brain tissue was dissociated on a shaker (50rpm) for 40 min at 35ºC. The digestion was stopped by addition of ice cold HBSS-. The tissue was centrifuged (200g, 3 min, RT), the supernatant completely aspirated and the tissue resuspended in isolation medium supplemented with 2% B27 and 2mM sodium-pyruvate (trituration solution). The tissue was allowed to sit in this solution for 5min. To obtain a single cell suspension the tissue suspension was triturated 10 times using first a 5ml serological pipette and subsequently three fire polished glass pipettes (opening diameter >0.5mm). After each trituration step the tissue suspension was allowed to sediment (approximately 1-2 min) and the supernatant (approximately 2ml), containing the cells, was transferred into a fresh tube. After each round of trituration 2ml of fresh trituration solution were added. To remove accidentally transferred undigested tissue bits, the collected supernatant was filtered through 70µm cell strainers into tubes that contained 90% isotonic Percoll (GE Healthcare, 17-0891-01, in 10xPBS pH7.2 (Lifetech). The final volume was topped

up with phenol-red free DMEM/F12 with HEPES (Gibco) and mixed to yield a homogenous suspension with a final Percoll concentration of 22.5%. The single cell suspension was separated from remaining debris particles by gradient density centrifugation (800g, 20min, RT, without break). The myelin debris and all layers without cells were discarded and the brain cell containing phase (last 2ml) and cell pellet were resuspended in HBSS+ and combined in a fresh 15ml tubes and centrifuged (300g, 5min, RT). The cell pellet was resuspended in red blood cell lysis buffer (Sigma, R7757) and incubated for 1min at RT to remove red blood cells. 10ml of HBSS+ were added to this cell suspension and spun down (300g, 5min, RT). The cell pellets were resuspended in 0.5ml modified Milteny washing buffer (MWB, 2mM EDTA, 2mM Na-Pyruvate, 0.5% BSA in PBS, pH 7.3) supplemented with 10ng/ml human recombinant insulin (Gibco). To this cell suspension 2.5µg mouse-anti-rat-A2B5-IgM antibody (Millipore, SI Tab. 4) were added for every 10 million cells. After 25 min incubation, gently shaking at 4ºC, 7ml of MWB were added. The solution was centrifuged (300g, 5min, RT) and the pellet resuspended in 80µl MWB supplemented with 20µl rat-anti-mouse-IgM antibody (Milteny, 130-047-302) per 10 million cells. The cells were incubated for 15 min, slowly shaking at 4°C. The secondary antibody was again washed out with 7ml MWB and the sample was centrifuged (300g, 5min, RT). The cell pellet was resuspended in 0.5ml and MACS was performed according to the recommendations of the supplier. Briefly, a MS column (Milteny, 130-042-201) were inserted into MiniMACS Separator (Miltenyi; 130-042-102) and pre-wet with 0.5ml MWB. Resuspended cells were put onto one MS column. Subsequently the column was washed three times using 500µl MWB for each wash. Finally, A2B5 positive cells were flushed out the column with 1ml pre-warmed, CO_2 and O_2 pre-equilibrated OPC medium.

Culture of adult oligodendrocyte progenitor cells

Isolated OPCs were seeded onto 12mm glass coverslips in 24 well plates (VWR) or into 96 well-plates (InVitro-Sciences) coated with PDL (Sigma). After isolation, OPCs were left to recover in OPC medium (60µg/ml N-Acetyl cysteine (Sigma), 10µg/ml human recombinant insulin (Gibco), 1mM sodium pyruvate (Gibco), 50µg/ml apo-transferrin (Sigma), 16.1µg/ml putrescine (Sigma), 40ng/ml sodium selenite (Sigma), 60ng/ml progesterone (Sigma), 330µg/ml bovine serum albumin (Sigma)) supplemented with b-FGF and PDGF (30ng/ml each, Peprotech). OPCs were incubated at 37ºC, 5% CO_2 and 5% O_2. The medium was completely exchanged to OPC medium with 20ng/ml bFGF and PDGF after overnight culture to remove

any dead cells. After 3d the cell culture medium was switched to promote further proliferation (OPC medium+20ng/ml bFGF and PDGF) or differentiation (OPCM + 40ng/ml T3). During differentiation or proliferation experiments 66% of the medium were replaced every 48h and growth factors or other small molecules were added fresh to the culture. The culture medium used was 500µl for cultures in 24 well plate wells and 150µl for cultures in 96 well plate wells. For differentiation assays the medium was in some instances supplemented with 40ng/ml thyroid-hormone (T3, Sigma), 50nM 9-cis retinoic acid (9cRA, Sigma), 1µM miconazole (Sigma, M3512) or 1.5µM benztropine (Sigma, SML0847). Otherwise used small molecules: 100µM metformin (Sigma, PHR1084-500MG), rotenone (Sigma, R8875), 1µM dorsomorphin (LC Laboratories, D-3197).

Mixed glia cell preparations and culture

Neonatal mice were decapitated after lethal injection with phenobarbital. The brains were then further processed as described for the isolation of rat OPCs. After the percoll gradient centrifugation cells were plated at 10,000 cells per well of a 96 well plate and cultured in 10% FBS (Gibco) in DMEM/F12. Cells were fed on alternate days.

Immunofluorescence for tissue sections

Mice received a lethal dose of pento-barbitol and were transcardially perfused with 4% paraformaldehyde (PFA) in PBS. The brains were removed and post-fixed for 2h at RT with 4% PFA. After a rinse in PBS the tissue was incubated in 20% sucrose solution (in PBS) overnight. The tissue was then imbedded in OCT-medium (TissueTek) and stored at -80ºC. 12 µm sections were obtained using a cryostat. Tissue sections were air dried and stored at -80ºC. Cryostat cut sections were dried for 45 min at RT. For antigen-retrieval the slides were submerged in preheated citrate buffer pH 6.0 (Sigma) in a water bath at 95ºC for 15 min. The slides were washed three times with PBS (5min, RT) and blocked in 0.3% PBST with 10%NDS for 1h at RT. Primary antibodies were diluted in 0.1% PBST with 5%NDS and incubated overnight at 4ºC. The slides were washed 3 times for 10min with PBS. Next, secondary antibodies in blocking solution were applied at a concentration of 1:500 for 2h at RT. Slides were washed 3 times with PBS for 10 min each, whereby the first wash contained Hoechst 33342 nuclear stain (2µg/ml,). The slides were mounted with coverslips using FluoSave (CalBiochem). Image acquisition was performed using a Leica-SP5 microscope (Leica) and LAS

software (Leica). Further image processing and analysis was performed using the ImageJ software package [34].

Immunofluorescence for cells

Cultured cells were rinsed with PBS before fixation with 4% PFA (10 min, RT). Subsequently, the cells were washed three times with PBS (5 min, RT, shaking). If permeabilisation was required, the cells were incubated with PBST (0.1% Triton-X-100 in PBS) for 20 min at RT. The samples were then blocked in PBS supplemented with 10% normal donkey serum (NDS). Primary antibodies were diluted in PBS with 5% NDS and incubated overnight at 4◦C in a humidified chamber. Excess antibodies were washed off with three washes in PBS (10 min, RT, shaking). The primary antibodies were then labelled with secondary antibodies (SI Tab. 4) diluted in PBS with 5% normal donkey serum. Again, excess antibody was washed off with three washes PBS (10 min, RT, shaking). If visualisation of nuclei was required the first wash contained 2µg/ml Hoechst 33342 (Sigma). If coverslips were used, they were mounted onto Polysine glass slides (VWR) in a drop of Fluosave (Calbiochem) and the slides were dried for at least 3h at RT in the dark. Images were taken with a Leica-SP5 (Leica) or Leica-SP8 (Leica) microscope. For 96 well plate assays cells were kept in PBS after staining. Further image processing and analysis was performed using the ImageJ software package [34].

EdU incorporation assays

For the EdU incorporation assay, 10µM EdU was added into the cell culture medium for five hours, followed by the protocol provided by the Click-iT Plus EdU Alexa Fluor 647 Imaging Kit (Thermo Fisher; C10640). Otherwise, in vitro tissue culture cells were fixed in 4% Paraformaldehyde (Thermo Fisher; 10131580) for 10 minutes at room temperature. The cells were then washed once in PBS (Thermo Fisher; BP3994) and then blocked in PBS with 0.1% Triton X-100 (Sigma; T8787) and 5% Donkey Serum (Sigma; D9663) for 30 minutes at room temperature. EdU detection was then performed by the protocol provided with the kit and immunostaining was performed subsequently as described above. For EdU incorporation assays *in vivo*, mice were injected i.p. with EdU (75µg/g of bodyweight in DMSO and sterile saline) 24h before perfusion fixation with PFA as described above. EdU detection was carried out according to the manufacturer's protocol and immune staining was performed

subsequently as described above. Fixed, fluorescent cells or slides were imaged using the Zeiss Axio Observer or the Leica TCS SP5 confocal microscope.

Induction of DNA damage using etoposide

To induce DNA damage etoposide (ETS) (abeam, ab120227) a topoisomerase II inhibitor was diluted at different concentrations ranging from 0.125 to 25µM in fresh OPC medium containing growth factors. OPCs were exposed to etoposide for 2h. The cells were washed once in pre-warmed DPBS to wash-out etoposide and the medium was then replaced with fresh OPC medium containing growth factors. The cells were cultured for a further 2h or 48h before cell viability was assessed or the degree of DNA damage was measured using comet assays.

Comet assay

For comet assays, a single cell gel electrophoresis-based assay for detecting DNA damage, approximately 5000 OPCs were resuspended in 100µl PBS and mixed with 300 µl 1% low melting point agarose (37ºC). Alternatively, when OPCs were cultured prior to the assay, the cells were detached using TrypLE 1x Select (Gibco) for 8 min at 37ºC. The comet assay was then performed as described [35]. Briefly, OPCs were centrifuged at 300g for 5 min. at room temperature and the cell pellet was resuspended with 100µl PBS and then mixed with 300µl molten low-melting point agarose pre-incubated at 37ºC. The cell-agarose suspension was then applied gently onto polysine slides that were pre-treated with 1% agarose and allowed to solidify at 4ºC. The slides were submersed in alkaline cell lysis buffer (0.3M NaOH, 100mM EDTA, 0.1% (w/v) N-Lauroylsarcosine (Sigma, 61745), 1.2M NaCl in ddH2O) for 16 hours at 4ºC in the dark. The slides were then electrophoresed in alkaline electrophoresis buffer (0.03M NaOH, 2mM EDTA, pH > 12.3, pre-chilled at 4ºC) for 25 min at RT with 1V/cm, whereby *cm* represents the distance between the electrodes. Finally, electrophoresed and propidium iodide stained DNA was visualized using a Zeiss Axiovision Fluorescence microscope (Carl Zeiss), and 50-100 nuclei per animal were visually scored according to published protocols [36]. To assess DNA repair the percent of DNA present in the tail of the comets was quantified using OpenComet software plugin (https://cometbio.org) in FIJI. Statistical significance was determined comparing respective damage categories between experimental groups by a two-tailed unpaired t-test. A significant result was assumed for $p<0.05$.

Viability assay

Calcein AM (ThermoFisher) dye was diluted in OPC medium containing growth factors to a concentration of 2µM. Old OPC medium was removed and the cells were washed once with pre-warmed DPBS. OPC medium containing Calcein AM was added to the OPCs and the cells were incubated for 20 min under normal culture conditions. The cells were then washed twice in PBS and fixed in 4% PBS. The cells were imaged on the same day using an InCell2000 microscope or a LeicaSP8 confocal microscope

RNA sequencing and downstream analysis

RNA was extracted according to the Directzol RNA MicroPrep Kit (Zymo Research; R2061) with the optional DNase treatment. RNA quality was assessed with a Bioanalyzer to ensure all samples had a RIN value of ≥ 8. DNA libraries were constructed using the SMARTer® Stranded Total RNA-Seq Kit - Pico Input Mammalian kit with multiplexed barcodes (Takara; 635005). 150 bp paired-end directional sequencing was performed on an Illumina HiSeq 4000.

Multiplexed samples were filtered, aligned to the rat UCSC rn6 assembly, normalized, and quantified using Trimmomatic, Hisat2, Stringtie, and Ballgown. Dendrogram clustering, t-distributed stochastic neighbor embedding, and heatmaps were generated in ipython notebook using the libraries pandas, matplotlib, numpy, seaborn, and scikit-learn. Gene Set Enrichment Analysis was performed using gseapy. Genes were ranked according to their log2 fold change and p-value. Reference pathway datasets (GO-Biological Processes, KEGG and Reactome Pathways) were downloaded from the MSigDB database v7.0 (released August 2019). Venn diagrams were created in R using the eulerr package. Scatterplots were created in R using the ggplot2 package.

RNA isolation and qRT-PCR

RNA was isolated from freshly purified OPCs or from cultured OPCs according to the Directzol RNA MicroPrep Kit (Zymo Research; R2061). All RNA samples were stored at -80˚ C prior to further processing. cDNA was generated using the QuantiTect Reverse Transcription Kit's according to the instructions of the manufacturer (Qiagen; 205310). For RT-qPCR, primers were used at a concentration of 400µM. The efficiency of each primer was greater than ~95%

as determined for each primer pair by serial dilutions of OPC cDNA. cDNA, primers, and the Syber Green Master Mix (Qiagen; 204141) were mixed as instructed by the manufacturer, and RT-qPCR and melting curve analysis were performed on Life Technologies' Quantstudio 6 Flex Real-Time PCR System. Fold changes in gene expression were calculated using the delta delta Ct method in Microsoft Excel. Statistical significance was determined using two-tailed unpaired t-tests assuming equal variances.

CRISPR/Cas9 mediated knockdown of MYC in vitro

Using Phusion polymerase (Thermo Fisher; F530S) a T7 promoter Cas9 PCR product was amplified from the AAV-CMVc-Cas9 plasmid (Addgene plasmid # 106431, Juan Ipiszua Belmonte's laboratory). The product was purified and used as a template to generate capped mRNA using the HiScribe mRNA kit with tailing (NEB, E2060S). All guide RNAs were designed using CHOPCHOP (https://chopchop.cbu.uib.no). DNA Templates containing a T7 promoter site for the generation of non-targeting and prkaa2 gRNAs were assembled by oligo annealing to a gRNA scaffold sequence using Klenow fragment (NEB, M0210S). gRNAs were then produced by *in vitro* transcription using T7 polymerase (NEB, M0251S). gRNAs were dephosphorylated using the Quick-CIP kit (NEB, M0525S) and were subsequently purified using RNA extraction columns (Zymo, R2060). Capped Cas9 mRNA and gRNAs were transfected into neonatal OPCs (seeded at 20,000 cells per 96 well to achieve approximately 80-90% confluency) using Lipofectamine LTX (Thermo Scientific, 15338100 , 0.4µl LTX, 0.1µl Plus reagent, 100ng Cas9 mRNA, 50ng gRNAs per 96 well in Opti-MEM, final volume 10µl). The medium was completely replaced after 16h. No potential off-target sites were predicted by CHOPCHOP (≤3 mismatches). Potential off-target sites (≥3 mismatches) were identified using CRISPOR (http://crispor.tefor.net). 4d after transfection, OPCs were lysed in in DNA Quick-Extract solution. Genomic targets sites were amplified by PCR using Phusion polymerase. To identify INDELs, PCR products were sequenced by Sanger sequencing and the chromatograms were analysed using TIDE (https://tide.nki.nl). All primer sequences can be found in Supplementary Information Table 2.

Generation of Nested CRISPR Plasmids

AAV-CMVc-Cas9 was a gift from Juan Belmonte (Addgene plasmid # 106431). pCAG-Cre-IRES2-GFP was a gift from Anjen Chenn (Addgene plasmid # 26646). pUCmini-iCAP-PHP.eB

was a gift from Viviana Gradinaru (Addgene plasmid # 103005). pSpCas9(BB)-2A-GFP (PX458) was a gift from Feng Zhang (Addgene plasmid # 48138). pHelper plasmid was a gift from the Cancer Research United Kingdom viral core facility.

U6 and gRNA sequences were ordered were ordered from Integrated DNA Technologies (see Supplementary Information Table 2).

Myc sequence was cloned from human iPS cells (gift from David Rowitch, Wellcome-MRC Cambridge Stem Cell Institute) and reverse transcribed with Protoscript II (NEB; M0368S). Using the AAV-CMVc-Cas9 plasmid backbone and AAV2 ITR sequences, we PCR amplified the IRES GFP, T2A, and Myc sequences using Phusion polymerase (Thermo Fisher; F530S) and products were gel extracted (Qiagen; 28704). The fragments were assembled using NEBBuilder HiFi DNA Assembly (NEB; E2621S) and sequences were confirmed with Sanger sequencing. Plasmids were purified with MIDI kit (Machery-Nagel; 740410.10).

Virus production protocol and in vitro, in vivo infection, and spinal cord lesions

AAV production and purification followed the previously described protocol (12). In brief, HEK293 cells were grown in 15mm plastic dishes and triple transfected with the pHelper plasmid, the PHP-EB capsid plasmid, and the transgene plasmid. Five days later cells were lysed and virus was isolated using Optiprep density gradient medium (Sigma; D1556) and ultra-centrifuged at 350000g. Viral layer was isolated and concentrated using Amicon Ultra-15 Centrifugal Filter Units (Sigma; Z648043-24EA). AAV titer was determined using SYBR green qPCR (See Supplementary Information Table 2). For in vitro studies, mixed glia cells grown in 10% FBS in DMEM/F12 were infected with 100,000 viral genomes per cell per viral particle. Media was changed 24 hours later and cells were left for 96 additional hours with media changes every 48 hours. For in vivo administration of the virus, mice were restrained and 5E11 viral genomes per virus were injected into the tail vein of 18-month-old C57/Bl6 mice.

Spinal cord lesions were created by injecting 1% lysolecithin in PBS into the ventral white matter tract of the spinal cord (see above). 21 days following tail-vein injection, mice were perfusion fixed.

For DNA/RNA extraction of CRISPR modified cells, DNA/RNA was isolated using TRIzol phase separation (Thermo Fisher; 15596026).

Modified mRNA transfection and small molecule treatment

Modified Myc, Sox2, and GFP mRNA with pseudo-UTP and methyl-CTP with a modified 5' Cap were ordered from Tebu Bioscience (L-7601-100, 05-0016, 05-0018). 48 hours following the plating of aged OPCs into 96 well plates, cells were transfected overnight with mRNA using Lipofectamine LTX or Lipofectamine Stem at the dosage recommended by the manufacturing guidelines (Thermo Fisher; 15338100). For these experiments 25ng of mRNA were transfected per 25,000 cells in a 96 well plate. Neonates were plated at 5,000 cells per well of a 96-well plate. After cultured overnight, cells were incubated in varying concentrations of 10058-F4 (Sigma).

Western Blot

Cells were lysed in IP lysis buffer (Thermo Scientific) supplemented with 1% Halt protease inhibitor (Thermo Scientific, 87786) for 10 min on ice. The lysates were spun down for 10min at 4C and 10, 000 g in a table top centrifuge. The supernatant was stored at 80C. Protein quantification was carried out using Pierce BCA protein assay kit (Thermo Scientific) measured with a Nano- drop2000. Equal amounts of protein (15-20mg) were loaded mixed with 4X BoltÒ LDS Sample Buffer (Thermo Fisher; B0007) and 10X Bolt reduction agent and boiled to 70C for 10min. Protein was run on Bolt 4%–12% Bis-Tris Plus Gels (Thermo Fisher; NW04120BOX) in Bolt MOPS SDS running buffer (Thermo Scientific, B0001) for 32min at 200V. Protein was transferred for 60min at 20V to a nitrocellulose membrane (Immobilon FL 0.45mm pore size, Millipore) membrane using the Mini Blot module (Thermo Scientific, B1000) and Bolt transfer buffer with 10% methanol and 1% Bolt antioxidant (Thermo Scientific, BT005) according to the manufacturer's instructions. Membranes were blocked in 50% Odyseey blocking buffer TBS (Li-Cor, 927-50100) in TBS. All pri- mary antibodies were used in a dilution of 1:1000 in 0.1%TBS-Tween with 50% Odyseey blocking buffer (TBS) in TBS. The mem- branes were incubated shaking in antibody solution overnight at 4C. The membranes were washed twice in 0.1% TBS-Tween. Secondary antibodies were added in a concentration of 1:10000 in 50% Odyssey blocking buffer in 0.1% TBS-Tween. Secondary antibodies were incubated at room temperature for 1h in the dark. The membranes were

washed three times in 0.1% TBS Tween. Fluorescent antibody signal was detected using the Odyssey (Li-Cor) and Image Studio v4.0 software.

Microarray analysis

Microarray raw data of adult and neonatal progenitors of oligodendrocytes, cuprizone-treated adult progenitors and control samples were acquired from GEO (accession no. GSE48872). Background subtracted median intensity (F532 Median - B532) were used. After removal of microarray controls (Dark/bright corner, SSC), probes which were not detected in all arrays and the outliers [37], we used 17906 unique probes (representing 12081 genes) for statistical analysis. Data were quantile normalized. Gene expression comparison between two groups (adult vs neonatal progenitors; cuprizone treated adult progenitors vs controls) was performed using Limma package [38]. Probes for which the difference between two groups were $\geq$2 fold and the FDR (Benjamini-Hochberg) adjusted p-value <0.05 were considered differentially expressed.

Transcription factor motif analysis

Transcription factor motifs were identified using HOMER2 software with standard settings using sequences within -2000 and +100bp of the transcriptional start site [39].

Quantification and statistical analysis

Statistical analysis

All statistical analysis was performed in GraphPad Prism (GraphPad Software, Inc.) or R. Prior to the analysis of parametric data we performed Shapiro-Wilk tests to ensure normality of the data. Biological replicates refer in cell culture experiments to cells isolated from an individual animal. For *in vivo* experiments biological replicates refer to data gathered from an individual animal. For data derived from the quantification of immunohistochemical staining, comparisons between two groups were performed with an unpaired t-test assuming two-tailed distribution and equal variances. In cases where more than two groups were compared to each other, a one-way analysis of variance (ANOVA) was performed assuming equal variances, followed by an appropriate post-test to compare individual groups. For qRT PCR

data two groups were compared to each other using unpaired two-tailed t-test. For all statistical tests, differences were considered significant at $p<0.05$.

Data and code availability

The RNA sequencing data of neonatal and aged oligodendrocyte progenitor cells (OPCs) generated during this study are available at GEO: GSEXXXXX

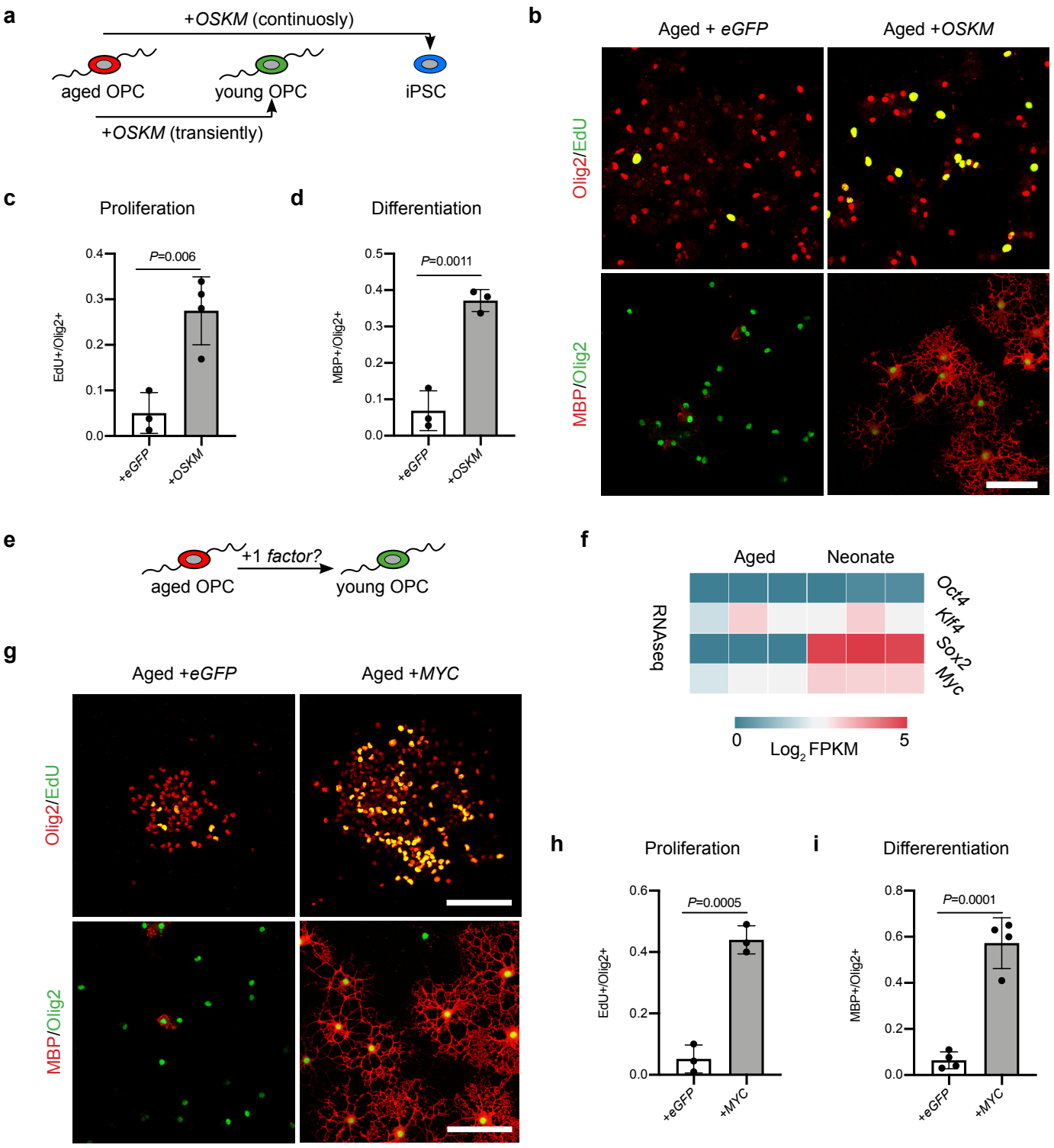
a
+OSKM (continuosly)
aged OPC
young OPC
iPSC
+OSKM (transiently)
b
Aged + eGFP
Aged +OSKM
Olig2/EdU
MBP/Olig2
c
Proliferation
P=0.006
EdU+/Olig2+
+eGFP
+OSKM
d
Differentiation
P=0.0011
MBP+/Olig2+
+eGFP
+OSKM
e
+1 factor?
aged OPC
young OPC
f
Aged
Neonate
RNAseq
Oct4
Klf4
Sox2
Myc
0
Log2 FPKM
5
g
Aged +eGFP
Aged +MYC
Olig2/EdU
MBP/Olig2
h
Proliferation
P=0.0005
EdU+/Olig2+
+eGFP
+MYC
i
Differerentiation
P=0.0001
MBP+/Olig2+
+eGFP
+MYC

Figure 1

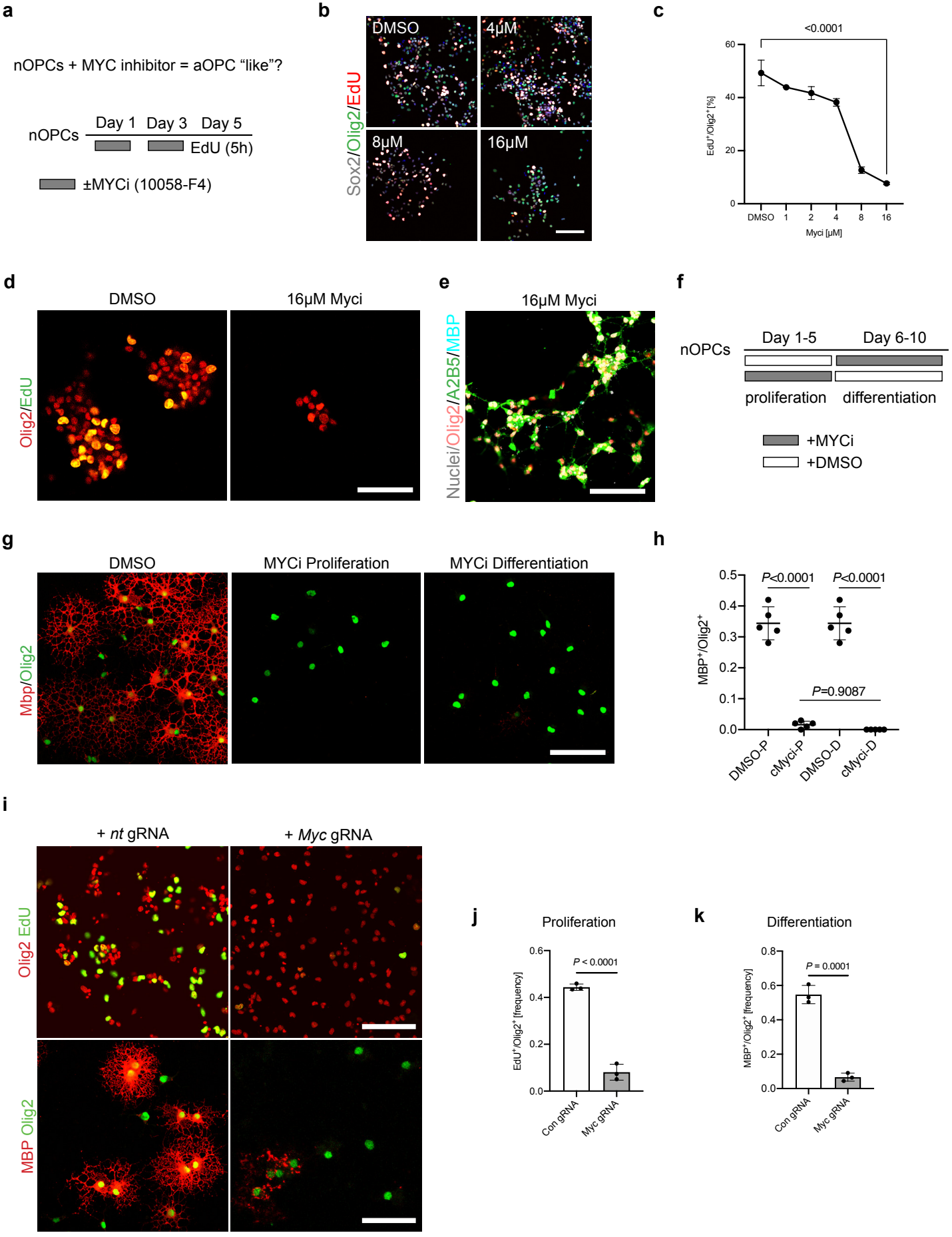
a
nOPCs + MYC inhibitor = aOPC “like”?
nOPCs
Day 1
Day 3
Day 5
EdU (5h)
±MYCi (10058-F4)
b
DMSO
4μM
8μM
16μM
Sox2/Olig2/EdU
c
<0.0001
EdU+/Olig2+ [%]
Myci [μM]
DMSO
1
2
4
8
16
d
DMSO
16μM Myci
Olig2/EdU
e
16μM Myci
Nuclei/Olig2/A2B5/MBP
f
nOPCs
Day 1-5
Day 6-10
proliferation
differentiation
+MYCi
+DMSO
g
DMSO
MYCi Proliferation
MYCi Differentiation
Mbp/Olig2
h
P<0.0001
P<0.0001
P=0.9087
MBP+/Olig2+
DMSO-P
cMyci-P
DMSO-D
cMyci-D
i
+ nt gRNA
+ Myc gRNA
Olig2 EdU
MBP Olig2
j
Proliferation
P < 0.0001
EdU+/Olig2+ [frequency]
Con gRNA
Myc gRNA
k
Differentiation
P = 0.0001
MBP+/Olig2+ [frequency]
Con gRNA
Myc gRNA

Figure 2

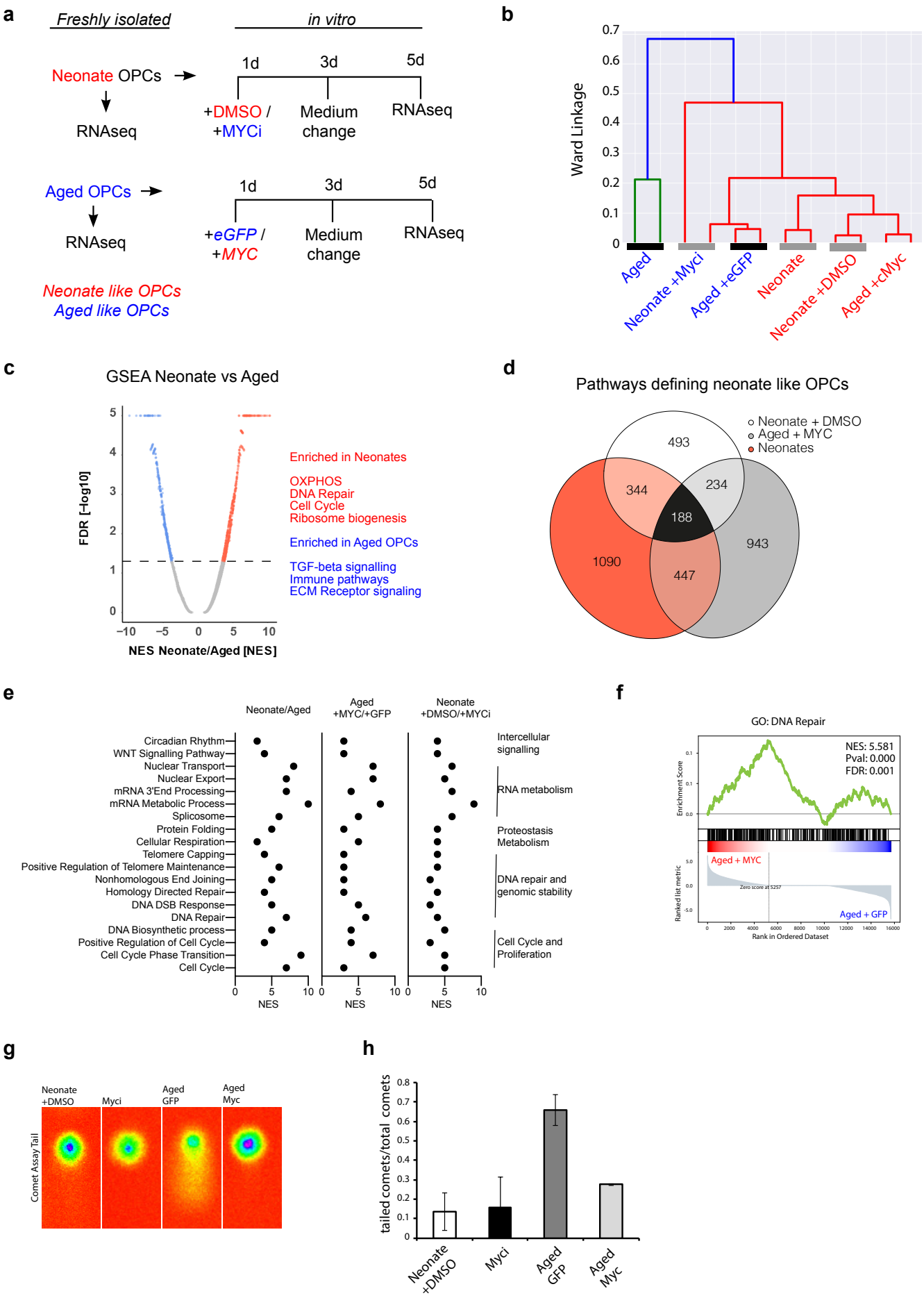
a
Freshly isolated
in vitro
Neonate OPCs
RNAseq
1d
3d
5d
+DMSO /
+MYCi
Medium
change
RNAseq
Aged OPCs
RNAseq
1d
3d
5d
+eGFP /
+MYC
Medium
change
RNAseq
Neonate like OPCs
Aged like OPCs
b
Ward Linkage
0.7
0.6
0.5
0.4
0.3
0.2
0.1
0
Aged
Neonate +Myci
Aged +eGFP
Neonate
Neonate +DMSO
Aged +cMyc
c
GSEA Neonate vs Aged
FDR [-log10]
5
4
3
2
1
0
−10
−5
0
5
10
NES Neonate/Aged [NES]
Enriched in Neonates
OXPHOS
DNA Repair
Cell Cycle
Ribosome biogenesis
Enriched in Aged OPCs
TGF-beta signalling
Immune pathways
ECM Receptor signaling
d
Pathways defining neonate like OPCs
Neonate + DMSO
Aged + MYC
Neonates
493
344
234
188
943
1090
447
e
Neonate/Aged
Aged
+MYC/+GFP
Neonate
+DMSO/+MYCi
Circadian Rhythm
WNT Signalling Pathway
Nuclear Transport
Nuclear Export
mRNA 3'End Processing
mRNA Metabolic Process
Splicosome
Protein Folding
Cellular Respiration
Telomere Capping
Positive Regulation of Telomere Maintenance
Nonhomologous End Joining
Homology Directed Repair
DNA DSB Response
DNA Repair
DNA Biosynthetic process
Positive Regulation of Cell Cycle
Cell Cycle Phase Transition
Cell Cycle
0
5
10
NES
Intercellular signalling
RNA metabolism
Proteostasis Metabolism
DNA repair and genomic stability
Cell Cycle and Proliferation
f
GO: DNA Repair
NES: 5.581
Pval: 0.000
FDR: 0.001
Enrichment Score
Aged + MYC
Aged + GFP
Ranked list metric
Rank in Ordered Dataset
g
Neonate
+DMSO
Myci
Aged
GFP
Aged
Myc
Comet Assay Tail
h
tailed comets/total comets
0.8
0.7
0.6
0.5
0.4
0.3
0.2
0.1
0
Neonate
+DMSO
Myci
Aged
GFP
Aged
Myc

Figure 3

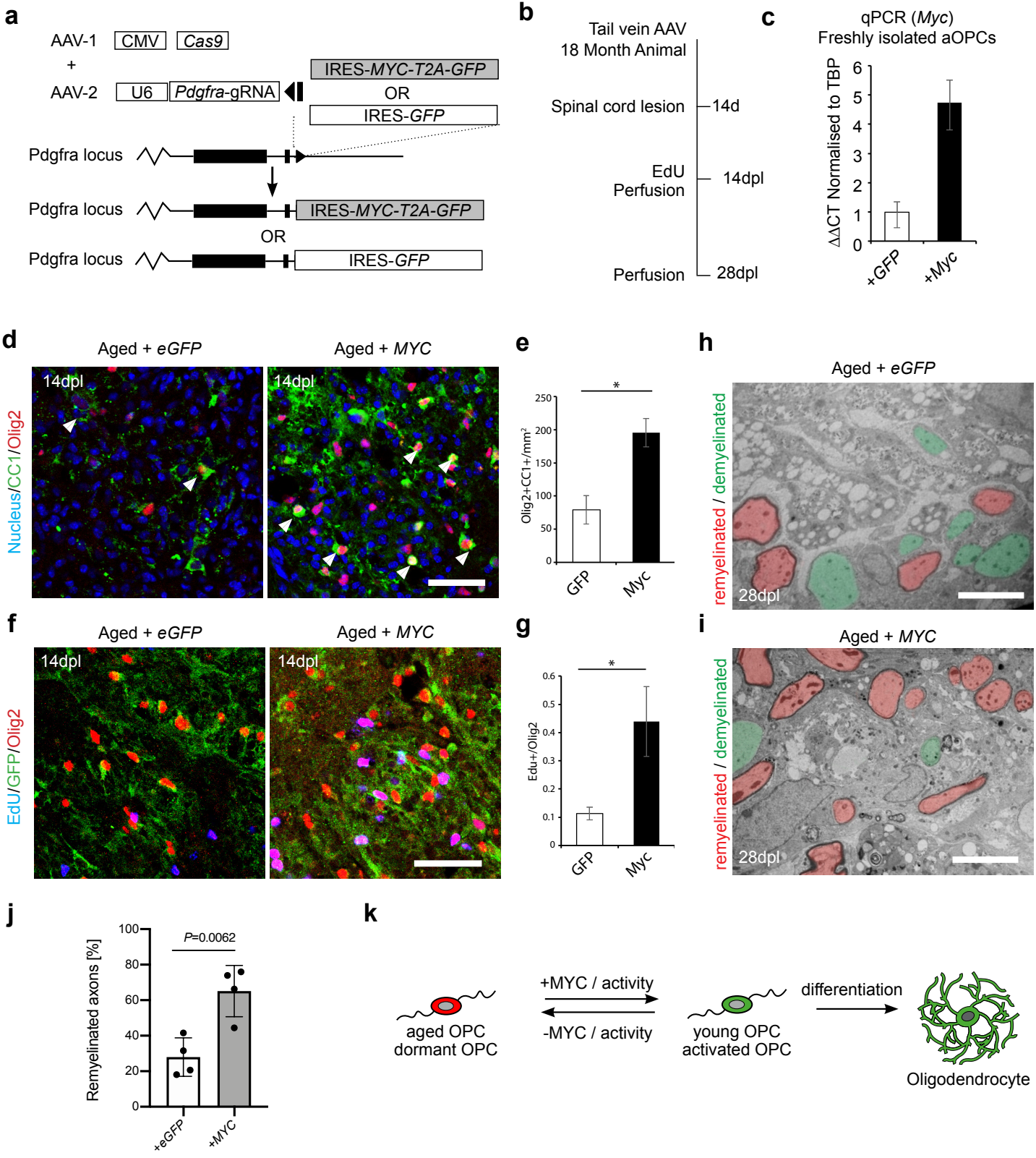
a
AAV-1
CMV
Cas9
+
AAV-2
U6
Pdgfra-gRNA
IRES-MYC-T2A-GFP
OR
IRES-GFP
Pdgfra locus
Pdgfra locus
IRES-MYC-T2A-GFP
OR
Pdgfra locus
IRES-GFP
b
Tail vein AAV
18 Month Animal
Spinal cord lesion
14d
EdU
Perfusion
14dpl
Perfusion
28dpl
c
qPCR (Myc)
Freshly isolated aOPCs
ΔΔCT Normalised to TBP
+GFP
+Myc
d
Aged + eGFP
Aged + MYC
14dpl
14dpl
Nucleus/CC1/Olig2
e
Olig2+CC1+/mm²
GFP
Myc
h
Aged + eGFP
remyelinated / demyelinated
28dpl
f
Aged + eGFP
Aged + MYC
14dpl
14dpl
EdU/GFP/Olig2
g
Edu+/Olig2
GFP
Myc
i
Aged + MYC
remyelinated / demyelinated
28dpl
j
P=0.0062
Remyelinated axons [%]
+eGFP
+MYC
k
aged OPC
dormant OPC
+MYC / activity
-MYC / activity
young OPC
activated OPC
differentiation
Oligodendrocyte

Figure 4